Article

Precise Measurements of the Temperature-Frequency Dependence of the Conductivity of Cellulose—Insulating Oil—Water Nanoparticles Composite

Pawel Zukowski [iD], Przemyslaw Rogalski, Tomasz N. Koltunowicz *[iD], Konrad Kierczynski [iD] and Vitalii Bondariev [iD]

Department of Electrical Devices and High Voltage Technology, Lublin University of Technology, 20-618 Lublin, Poland; p.zhukowski@pollub.pl (P.Z.); p.rogalski@pollub.pl (P.R.); k.kierczynski@pollub.pl (K.K.); v.bondariev@pollub.pl (V.B.)
* Correspondence: t.koltunowicz@pollub.pl; Tel.: +48-81-538-47-13

Abstract: This article presents direct σDC and alternating σ(f) current conductivity measurements obtained by the frequency domain spectroscopy (FDS) method on cellulose-transformer oil–water nanoparticle composite with a moisture content of $(5.0 \pm 0.2)\%$ by weight in a temperature range from 293.15 to 333.15 K with step of 8 K. The uncertainty of temperature maintenance during measurements was below ± 0.01 K. The sample was prepared for testing in a manner as close as possible to the cellulose insulation moisturizing process in power transformers. For the analysis of the results obtained, a model of alternating and direct current hopping conductivity was used, based on the quantum phenomenon of electron tunneling between the potential wells and nanodrops of water. It was observed that on the d(logσ)/d(logf)-derived waveforms there was a clear low-frequency maximum, and a tendency to reach the next maximum in the high-frequency area was visible. On this basis it was established that the increase in conductivity takes place in two stages. It was found that the position of σ(f) waveforms in the double logarithmic coordinates is influenced by the temperature dependence both of the conductivity and of the relaxation time of the conductivity. These relationships are described with the appropriate activation energies of the conductivity and relaxation time of conductivity. Based on the analysis of experimental data using Arrhenius diagrams, average values of the activation energy of conductivity $\Delta W\sigma \approx (0.894 \pm 0.0134)$ eV and the relaxation time of conductivity $\Delta W\tau\sigma \approx (0.869 \pm 0.0107)$ eV were determined. The values were equal within the limits of uncertainty and their mean value was $\Delta W \approx (0.881 \pm 0.0140)$ eV. Using the mean value of the activation energy, the frequency dependence of conductivity, obtained at different temperatures, was shifted to 293.15 K. For this purpose, first the waveforms were shifted along the horizontal and then the vertical axis. It was found that after the shift the σ(f) waveforms for the different temperatures overlap perfectly. This means that the shape of the frequency dependence of the conductivity is determined by the moisture content of the pressboard. The position of the waveforms in relation to the coordinates is determined by the temperature relationships of the conductivity and the relaxation time of the conductivity.

Keywords: power transformer; pressboard; mineral oil; moisture; conductivity; activation energy

1. Introduction

To assess the state of insulation in power transformers, the dielectric loss factor or resistance measurements determined using the absorption coefficient R60/R15 [1,2] are mostly used. New methods consisting of the measurement and analysis of relaxation phenomena in the insulation of transformers over a wide range of time or frequency are also applied. These methods make it possible to precisely determine the amount of water accumulated in the pressboard or to estimate the degree of the insulation degradation. To test the moisture content of power transformer insulation, diagnostic methods based on

relaxation changes in the time domain using the recovery voltage method (RVM) [3–6] and polarization depolarization current (PDC) method [7–10] are used. In the frequency domain, however, the values of the loss factor tgδ and system capacity at low frequencies are determined using the frequency domain spectroscopy (FDS) method [11–15].

The global literature also includes research related to influences of water on aging characteristics of insulation paper [16] and adsorption of mineral oil and water by insulation paper [17]. New and improved methods for measuring the moisture content of mineral-oil-impregnated cellulose pressboard have been described [18–20].

The most common methods used to determine the moisture content of cellulose insulation in power transformers are electrical methods using direct or alternating current measurements. To properly analyze the test results of transformers, so-called standard dependencies are necessary, and are determined for different moisture levels and temperatures of insulation. The standard dependencies, as a rule, are performed in laboratories on the basis of paper or electrotechnical pressboard dried under vacuum, humidified in air, and then impregnated with insulating oil [21–24]. In the paper [25], on the basis of analysis of the test results of moisturized paper impregnated with insulating oil, it was found that water accumulates in cellulose fibers in the form of a nanodrops with a diameter of about 2.3 nm, containing about 220 water molecules each. In a number of papers, measurements of alternating current properties of insulation parameters have been made to shorten the time of their execution—usually three points per decade and sometimes even eliminating measurements in the lowest frequency range [26–29].

The aim of this study was to precisely determine the standard dependencies for direct and alternating current conductivity of the electrotechnical pressboard, moistened in a manner as close as possible to the process of moistening the cellulose in power transformers. For this purpose, the number of measuring points per decade was applied several times greater than in previous studies. A climate chamber was used for the tests, for which the uncertainty of temperature maintenance and measurement was below ±0.01 K. The measurements were made in the temperature range from 293.15 to 333.15 K with a step of 8 K. A sample with water content (5.0 ± 0.2)% by weight was tested. The use of such a high moisture content in tests is connected with the fact that exceeding the value of about (5.0 ± 0.2)% of the weight may lead to the failure of the transformer [30–32]. The analysis of the obtained results was carried out with the use of the direct (DC) and alternating (AC) current hopping conductivity model developed on the basis of the quantum-mechanical electron tunneling phenomenon [33–37]. This model has proven to be excellent for the constant and alternating current analysis of the conductivity of a cellulose, mineral oil, and water nanoparticle composite prepared in a traditional way, i.e., by means of drying, humidifying, and then impregnation [37].

2. Foundations for the Analysis of Constant and Alternating Current Material Parameters of a Composite of Cellulose, Transformer Oil, and Water Nanoparticles

2.1. Conductivity

Alternating current testing of the conductivity of insulating materials is carried out in a parallel RC substitution scheme. The angle of phase shift between the conduction current and the shift current is $-90°$. This means that in real dielectrics the phase shift angle φ is within $0° \geq φ \geq -90°$.

To determine the alternating current parameters of electrical systems or insulating materials, meters are used, which are called admittance meters. In the case of alternating current transformer insulation tests, these meters are often called FDS meters. These meters perform, in a RC parallel scheme, measurements of two basic values that describe systems with passive elements. For insulating materials these are the values of phase shift angle φ and admittance Y. The angle of phase shift, as a rule, is calculated on the basis of the difference of angles for which there are zero values on the sine waveforms of current and

voltage. The value of admittance is determined on the basis of the quotient of the current and supply voltage amplitudes [38]:

$$Y = \frac{I}{V} \tag{1}$$

where: Y—admittance; V—supply voltage amplitude; I—current amplitude.

FDS meters on the basis of their own software calculate the resistance Rp and the capacity Cp in the RC parallel substitution scheme. Using these values and the geometric dimensions of the insulation, it is possible to calculate the alternating current conductivity and permittivity of the oil impregnated pressboard:

$$\sigma = \frac{d}{R_p S} \tag{2}$$

$$\varepsilon' = \frac{C_p d}{\varepsilon_0 \cdot S} \tag{3}$$

where: S—surface area of the measuring capacitor lining, d—plate thickness.

Material parameters of real dielectrics, conductivity, and dielectric permeability determine the values of conduction and displacement currents density which, according to the second Maxwell equation, are sources of magnetic field [33]:

$$\nabla \times \vec{H} = \vec{j}_R + \vec{j}_C = \sigma \vec{E}_0 \sin(\omega t) + \omega \varepsilon' \varepsilon_0 \vec{E}_0 \sin\left(\omega t - \frac{\pi}{2}\right) \tag{4}$$

where: $\vec{H}$—magnetic field strength vector, $\vec{j}_R$—conduction current density, $\vec{j}_C$—displacement current density, E_0—electric field amplitude, $\omega = 2\pi f$—circular frequency, f—frequency, t—time, σ—conductivity, ε—relative dielectric permittivity, ε_0—vacuum dielectric permittivity.

Using the FDS method it is possible to obtain the frequency and temperature dependence of the conductivity of a electrotechnical pressboard, insulating oil, and water nanodrop nanocomposite, and to analyze the relaxation mechanisms occurring in the insulating material investigated.

2.2. Quantum Mechanics Components

For the analysis of alternating current conductivity in the article, a model of alternating and direct current hopping conductivity was used. The model is based on the quantum mechanical phenomenon of electron tunneling between nanoparticles placed in a low conductivity matrix. This condition is satisfied by a composite with the composition of an electrotechnical pressboard impregnated with insulating oil containing nanodrops of water. In relation to such a composite, the model assumptions can be presented as follows [37]:

- Nanodrops of water form potential wells of nanometer dimensions in the composite. The average distances between these are also nanometric. The barrier between the nanodrops is an insulating material.
- Electrons can tunnel between three-dimensional potential wells. The probability of tunneling into a unit of time is determined by the formula [39,40]:

$$P(T) = P_0 \exp\left(-\frac{\beta_r}{R_B} - \frac{\Delta W}{kT}\right), \tag{5}$$

where: P_0—numerical factor; r—average distance between the nearest nanodrops; β—coefficient with the value $\beta \approx (1.75 \pm 0.05)$ [41], R_B—jumping electron wave function radius of location (Bohr radius); ΔW—activation energy; k—Boltzman constant; T—temperature.

- The hopping conductivity takes place in a weak electric field, which does not change the value of jump probability of the $P(T)$ electrons but only leads to the formation of their jump asymmetry, taken into account by the Debye factor [42]:

$$\exp\left(\pm\frac{erE_0}{kT}\right),\tag{6}$$

where: e—electron charge, r—average distance between potential wells; E_0—electric field amplitude; k—Boltzman constant; T—temperature.

From formulas (5) and (6) the formula for DC conductivity can be derived for the case of tunneling between the potential wells—adjacent, (see for example [39]):

$$\sigma(r, T = const) = \sigma_0 exp\left(-\frac{\beta r}{R_B} - \frac{\Delta W}{kT}\right).\tag{7}$$

In the area of weak fields, defined by inequality:

$$e \cdot r \cdot E \ll k \cdot T,\tag{8}$$

conductivity does not depend on electric field strength.

After jumping (tunneling) of the electron from one well to another, an electric dipole is formed, which results in additional polarization of the material [34].

The jump causes the formation of current density j_0, described by the formula:

$$j_0 = \sigma_0 E \sin \omega t,\tag{9}$$

where: ω—circular frequency, σ_0—conductivity value.

To determine the value of σ_0, entering into formula (9) and subsequent formulas, solutions proposed, for example, in the paper [43], can be used.

After tunneling, the electron remains in the second well for time τ, called relaxation time. After time τ, two scenarios of further jumps are possible. First, the electron can jump in the direction opposite to the electric field to the third well (move away from well one). The probability of such a jump is $p << 1$. As a result of such a jump, a flow of DC or low-frequency current of density is observed:

$$j_+ = p\sigma_0 E \sin \omega(t - \tau).\tag{10}$$

In the case of the second scenario, the electron returns from well two to well one. The probability of return is $1 - p \approx 1$. This causes the flow of current at higher frequencies of density:

$$j_- = -\sigma_0 E(1 - p) \sin \omega(t - \tau).\tag{11}$$

The total current density is given by the formula:

$$j = j_0 + j_+ + j_- = \sigma_0 E[\sin \omega t + p \sin \omega(t - \tau) - (1 - p) \sin \omega(t - \tau)].\tag{12}$$

Formula (12) shows that the j_+ and j_- components are phase shifted in relation to j_0. This means that the resultant current density has both real and imaginary components. The actual current density component, related to material conductivity, is:

$$j_r = \sigma_0 E(1 - \cos \omega\tau + 2p \cos \omega\tau) \sin \omega t.\tag{13}$$

Formula (13) shows that for direct or low-frequency current ($\omega \to 0$) the current density value does not depend on the frequency and amounts to:

$$j_r = 2p\sigma_0 E \sin \omega t.\tag{14}$$

In this case, the phase shift angle is close to zero. In the high frequency area, the current density is also not dependent on the frequency:

$$j_r = \sigma_0 E \sin \omega t. \tag{15}$$

As is well-known, current density and conductivity are linked by the formula:

$$j = \sigma E. \tag{16}$$

Formulas (14) and (16) show that the DC or low-frequency conductivity for electron tunneling amounts to:

$$\sigma_{DC} = 2p\sigma_0. \tag{17}$$

On the other hand, in the high frequency area:

$$\sigma_H = \sigma_0. \tag{18}$$

Formulas (17) and (18) show that the high-frequency conductivity is $1/(2p)$ times higher than the DC conductivity. The value of p included in formulas (10)–(17) can be determined from the experimental course $\sigma_{(f)}$. The analysis of formulas (17) and (18) shows that p is the quotient of the conductivity values in the low σ_{DC} area and high σ_H frequency:

$$p = \frac{\sigma_{DC}}{2\sigma_H}. \tag{19}$$

In the area of intermediate frequencies, where $\omega\tau < 1$, there is an increase in current density and its dependence on the frequency can be described following the Mott's formula [39]:

$$j_r \sim f^{\alpha(f)}, \tag{20}$$

where: $\alpha(f)$—frequency factor.

According to the Mott model [39], parameter $\alpha \leq 0.8$ does not depend on frequency. From the model of the hopping conductivity for composites of pressboard, mineral oil, and water nanodrops [37], it follows that $\alpha_{(f)}$ is a function of frequency. In the area of intermediate frequencies, the phase shift angle is $0° > \varphi > -90°$.

As established in papers [25,29,37,44,45], the relaxation time value should depend on the distance between the nearest potential wells, generated by the nanodrops of water. In this work a relaxation time formula was derived for the conductivity of electron tunneling:

$$\tau = \tau_0 \exp\left(\frac{\beta \cdot r}{R_B}\right) \cdot \exp\left(\frac{\Delta W}{kT}\right), \tag{21}$$

where: τ—relaxation time; τ_0—unknown numerical factor; β—a numerical factor, the value of which, according to [41] is $\beta \approx (1.75 \pm 0.05)$; r—distance over which the electron tunnels; R_B—Bohr radius of the tunneling electron; ΔW—activation energy of relaxation time.

Formula (21) shows that the relaxation time depends on the distance over which the electron tunnels. In our case it is the distance between adjacent nanodrops. Current conductivity in composites containing nanoparticles is carried out through percolation channels, connecting measuring electrodes. In a 1 mm percolation channel, the number of water nanodrops and the number of distances between them is in the order of 105. The nanodrops in the pressboard are distributed at random. The central limit claim shows that the probability distribution of the distance between nanodrops is approximately normal (Gaussian distribution). This means that there are pairs of adjacent wells in the percolation channel, distances between which are both smaller and larger than the average. Formula (21) shows that for a pair of wells with a distance less than the average, the relaxation time is less than the average. For a pair of adjacent wells with a distance greater than the average, the relaxation time is greater than the average. As a result, in a composite

of electric pressboard, mineral oil, and water nanoparticles a probability distribution of the relaxation times occurs.

The probability distribution of relaxation times should be determined for positive values τ. The occurrence of negative τ values would mean that the electron will return from well two to well one even before tunneling from well one. Such conditions, i.e., only positive values of relaxation time τ, correspond, among others, to Landau's probability distribution in the approximation of Moyal [46]:

$$F_L(\tau) = \frac{1}{\sigma_m\sqrt{2\pi}} \exp\left(-\frac{\tau - \tau_m}{2\sigma_m} - \frac{1}{2}\exp\left(-\frac{\tau - \tau_m}{\sigma_m}\right)\right), \qquad (22)$$

where: σ_m—standard deviation; τ_m—expected relaxation time value.

Taking into account the distribution of Landau's formula (13) on the frequency dependence of conductivity, we can write it in the form:

$$\frac{\sigma(\omega)}{\sigma_0} = \int\limits_0^\infty F_L(\tau)(1 - \cos\omega\tau + 2p\cos\omega\tau)\sin\omega t d\tau. \qquad (23)$$

From formula (23), the frequency dependence of alternating current conductivity was calculated using numerical methods taking into account the Landau probability distribution. The $\sigma_{(f)}$ dependencies for the probability value p from 10^{-6} to 0.5 were obtained with a very small step of change in the p value. Figure 1a presents the $\sigma_{(f)}/\sigma_0$ dependencies, and Figure 1b the frequency coefficient $\alpha_{(f)}$ dependencies for seven selected probability values p from 0.0001 to 0.1. As can be seen from Figure 1a, in the low frequency area $\sigma_{DC(f)}$ = const. A further increase in frequency causes a rapid increase in conductivity. The maximum slope of the rising section decreases with an increase in the jump probability value p. In the high frequency area, where $\tau m f > 0.1$, consequently $\sigma_{H(f)}$ = const.
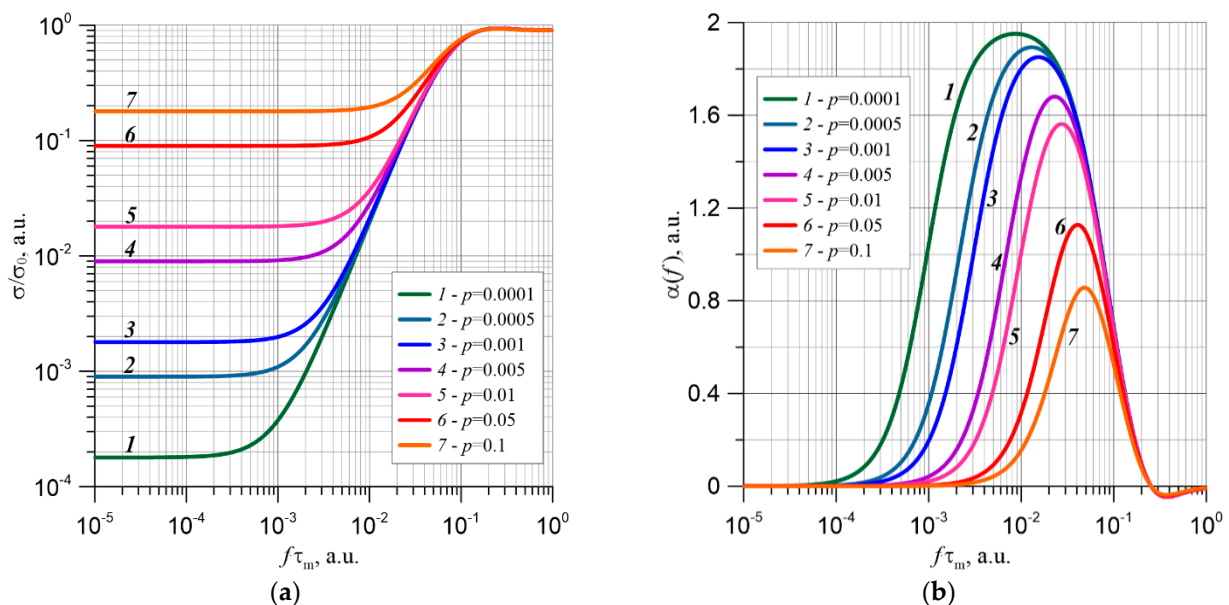

Figure 1. Relative conductivity dependences in the function of frequency f and time τ_m product for materials with a stepping exchange of charges (**a**) and dependences of the frequency coefficient $\alpha(f)$ (**b**). Computer simulation for p from 0.0001 to 0.1.

The hopping conductivity model discussed above describes, as shown in Figure 1, the occurrence in the low frequency area of DC conductivity, the value of which does not depend on frequency. With a further increase in frequency there is a rapid increase in

conductivity. Then there is a stabilization of the conductivity at a level much higher than the value of DC conductivity.

Figure 1b shows the frequency dependence of the coefficient $\alpha_{(f)}$ entering into formula (20). The coefficient $\alpha_{(f)}$ shows the slope of $\sigma_{(f)}$ in double logarithmic coordinates. The maximum position $\alpha_{(f)}$ is at the frequency at which the fastest increase in conductivity occurs. Figure 1b shows that $\alpha_{(f)}$ in the low frequency area is zero and the conductivity is constant. As the frequency increases, an increase in $\alpha_{(f)}$ is observed until the maximum is reached. As the frequency increases further, $\alpha_{(f)}$ decreases to zero. The waveforms presented in Figure 1b show that as the probability of jumping p increases, the maximum value $\alpha_{max}(f)$ decreases and the position of maximum moves to the higher frequencies. Figure 1a,b on the horizontal axis show values of ($f\,\tau m$). Comparison of the experimental frequency dependence $\alpha_{max}(f)$ and the numerical determination $\alpha(f\,\tau m)$ shown in Figure 1b allows determination of the value of the expected relaxation time τm entering into formulas (22) and (23). To do this, a relationship is chosen from a family of waveforms $\alpha(f\,\tau m)$ defined numerically, the maximum value for which is equal to the maximum experimental curve:

$$\alpha_{\max}(f)_m = \alpha_{\max}(f\tau_m). \tag{24}$$

Then, from the numerical determination, the maximum position ($f\,\tau m)max$ is determined and, from the experimental determination, the frequency $fmax$ at which the maximum value $\alpha max(f)$ occurs is determined. Based on these data, the expected relaxation time is determined from the formula:

$$\tau_m \;=\; \frac{(f\tau_m)_{max}}{f_{max}}, \tag{25}$$

where: ($f\,\tau m)max$—position of the maximum for the curve $\alpha(f\,\tau m)$ determined numerically; $fmax$—frequency at which the maximum value of $\alpha max(f)$ of the experimental curve occurs.

In a number of works, the model of hopping conductivity (electron tunneling) at direct and alternating current for composites containing nanoparticles of metallic phase in dielectric matrices was verified (see, for example, Ref. [35,36]). In this work it was proven that there is both qualitative and quantitative agreement of experimental results with the model of DC and AC hopping conductivity. This model has been successfully used to analyze frequency and temperature dependence of alternating current conductivity of the electrotechnical pressboard, insulating oil, and nanodrops of water composite for the moisture content range from 1% to 4% of weight [37].

The analysis of the hopping conductivity (electron tunneling) model at direct and alternating current has shown that frequency courses of conductivity are determined by two basic parameters—relaxation time τ and jump probability p.

The value of p determines the ratio of conductivity values in high and low frequency areas, described by formula (19). The lower the value of the jump probability p, the greater the ratio. The value of the relaxation time determines the position of the frequency for which the fastest increase in conductivity occurs and the frequency factor $\alpha(f)$ reaches its maximum.

3. Materials and Methods

3.1. Materials

The use of the FDS method to determine the moisture content of solid insulation of power transformers requires reference relationships, defined for different water contents and temperatures. For this purpose, laboratory tests are performed on paper and electrotechnical pressboard of different water content. To date, samples for laboratory tests were prepared using the following technology. The pressboard was vacuum dried at a temperature of about 353 K for up to two or three days. Then its mass was measured and the mass which should be obtained by the sample after it has been moistened to a given value was calculated. The sample was left in the atmospheric air until it reached its

calculated mass. After reaching the set mass, the sample was immersed in transformer oil for impregnation.

In transformers, the vacuum-dried pressboard is vacuum impregnated with transformer oil. During many years of operation, moisture penetrates into the transformer and dissolves in the oil. The oil supplies the moisture to the cellulose insulation, where it accumulates because its solubility in cellulose is about 1000 times higher than in oil [47]. This means that the natural process of moistening the cellulose in the transformer is fundamentally different from the way samples are moistened for laboratory tests. Transformers are first subjected to drying and vacuum impregnation. Then, slow (over many years) absorption of moisture into the oil-impregnated pressboard takes place. In the samples for laboratory tests, the moisture penetrates from the atmosphere into the dried unimpregnated pressboard. After moistening, impregnation is carried out in atmospheric pressure, not in vacuum.

In the work for the production of samples, a method of moisturizing the pressboard as close as possible to the natural moisturization of the pressboard in power transformers was used. For this purpose, three identical plates were cut out of the pressboard. Two of them were vacuum-dried and then moisturized in atmospheric air and immersed in insulating oil for impregnation. These tiles served as sources of moisture. The third tile, intended for testing, was vacuum-dried, and while left in the vacuum, it was flooded with insulating oil, where it was impregnated. After vacuum impregnation, the third plate was placed in an oil vessel between two previously moistened plates, as sources of moisture. Moisturization of the dried and vacuum impregnated panel intended for testing was carried out in the same way as moisturizing the pressboard in power transformers, namely, moisture from previously moisturized pressboard plates diffused into oil. The oil transferred the moisture to the impregnated dry panel, where it was absorbed by the cellulose. The time of moisturizing the tile to be tested was over a year and a half.

For the tests presented in this paper, a sample of pressboard with moisture content $(5.0 \pm 0.2)\%$ by weight was prepared as described above. In the work, Weidman's electrotechnical pressboard and Nynas' transformer oil were used, with a moisture content of several ppm, dedicated to building insulation of power transformers.

3.2. Methods

The diagram of the test stand used in the work for the measurement of alternating current parameters of the electrotechnical pressboard, insulating oil, and nanodrops of water composite is presented in works [48,49]. The main component of the stand is a three-electrode measuring system. Measuring and voltage electrodes are used to measure the cross-current intensity, flowing perpendicularly to the surface of the pressboard sample. The protective electrode is used to discharge the surface current to earth. The pressboard plate, moistened in a manner as close as possible to that of permanent insulation in power transformers, is placed between the electrodes. A metallic voltage electrode, made in the form of a 50 mm high cylinder with a diameter of 160 mm, presses a sample of the pressboard to the measuring electrode. The three-electrode measuring system and the sample is placed in a hermetic vessel and flooded with a small amount of oil, so that its surface is located above the pressboard plate. The measuring vessel with the condenser and the pressboard plate is placed in a climate chamber.

To maintain the temperature precisely, the climate chamber was developed and manufactured. The chamber was equipped with a proportional-integral-differential (PID) regulator electronic control system, forced air circulation and a chilled air source. A time of approx. 5 h was needed to reach and stabilize the preset temperature of the measuring capacitor. This is due to the high mass of the measuring capacitor together with the vessel and oil. Once the set temperature has been reached, the climate chamber maintains it for many hours. The temperature of the measuring capacitor was monitored with the PT 1000 sensor and AGILENT 34970A temperature meter (Agilent Technologies, Santa Clara, CA, USA) and recorded in computer memory every 1 s. Based on the recording of the

measurement results within thirty hours (108,000 measuring points), an uncertainty of measurement of temperature type A was determined, the value of which did not exceed ± 0.01 K. For the measurement of DC and AC properties, a Dirana meter—FDS-PDC dielectric response analyzer (OMICRON Energy Solutions GmbH, Berlin, Germany)—was used. This meter allows for DC and AC measurements in the frequency range from 0.0001 to 5000 Hz at voltages up to 200 V.

As a rule, in FDS alternating current tests, measurements are made at three points per decade [11,50–52]. In this way, tests of power transformers have also been performed [53–58]. This is due to the very highly time-consuming characteristic of measurements at ultra-low frequencies. For example, a single period of sinusoidal voltage at 0.0001 Hz is equal to 10,000 s, which is about 2.77 h.

In our tests of the pressboard, moistened in a manner as close as possible to that of solid insulation in transformers, alternating current measurements in the frequency range from 10^{-3} to 5000 Hz were made at 10 measurement points per decade. In the frequency range from 10^{-4} to 10^{-3} Hz, 5 points per decade were recorded. This lengthened the testing time and also improved the accuracy of reference characteristics' determination. To further improve the accuracy of reference characteristics' determination, the number of measurement temperatures was extended. Measurements were performed at six measurement temperatures: 293.15, 301.15, 309.15, 317.15, 325.15, and 333.15 K. This had a positive impact on the accuracy of the determination of the activation energy of the direct and alternating current conductivity of the oil-impregnated pressboard.

The work of the meters and the climatic chamber was controlled by a computer program, which allows for remote control of the stand (setting of the measurement mode—direct or alternating current—supply voltage values, measurement temperature) and recording of measurement results.

Tests of direct and alternating current conductivity of the pressboard, moisturized in a manner as close as possible to the moisturization of solid insulation in power transformers, were performed in the following manner. Measurements were started from the lowest temperature of 293.15 K. After reaching and stabilizing the set temperature, the measuring capacitor was supplied with DC voltage of VDC = 100 V. The Dirana meter raised the voltage to the set value gradually within about 8 s. After reaching the preset voltage value, the value of the volume current was recorded. Current and capacitor temperature values were recorded and stored in the computer memory once per second. Recording of DC current intensity lasted for two hours (7200 s). After the DC measurements were completed, alternating current measurements were started. This was done from the highest frequency of 5000 Hz. After measurements were taken at the first frequency, the computer program changed the frequency to the next. This procedure was repeated until the measurement was performed at the lowest frequency of 0.0001 Hz. After the measurements were completed at the temperature of 293.15 K, the next temperature was set, and after its stabilization the next cycle of electrical measurements was performed.

4. Temperature Influence on Constant and Alternating Current Conductivity Values

The study examined a sample of pressboard moisturized to the water content of $(5.0 \pm 0.2)\%$ by weight in a manner as close as possible to that of pressboard moistened in power transformers. Such a high moisture content was selected due to the fact that its accumulation in the solid insulation above 5% of weight might lead to catastrophic failure of the transformer [59–61]. Figure 2 shows the time dependence of the volume–current intensity for measuring temperatures from 293.15 to 333.15 K with a step of 8 K. As the time increases, the current intensity, determined at each temperature, decreases and then stabilizes. From the value of the determined current intensity, the value of DC conductivity was calculated using formula (16). Figure 2 shows that, with an increase in temperature from 293.15 to 333.15 K, the determined current intensity, i.e., also the conductivity, increases about 50 times. On the basis of the temperature dependence of DC conductivity, the Arrhenius diagram presented in Figure 3 was drawn. The linear

approximation of the experimental results by the method of smallest squares showed its very high quality. This is evidenced by the value of the determination factor $R^2 = 0.9992$, which is very close to unity. On the basis of the approximation formula obtained with the use of numerical methods, the activation energy of the DC conductivity of the pressboard, moistened in a manner as close as possible to that of the solid insulation in power transformers, was determined. Its value was $\Delta W_{DC} = 0.8022$ eV.
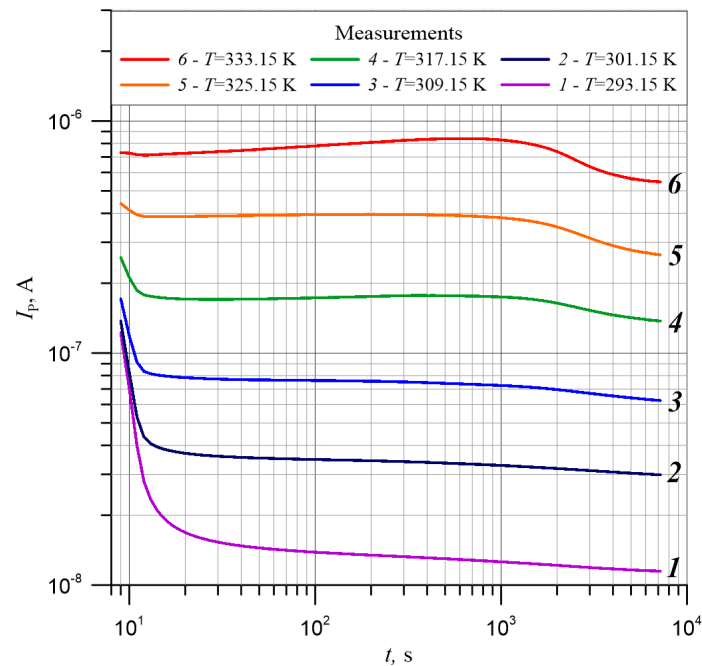

Figure 2. Time dependence of volume–current intensity of a composite of cellulose, transformer oil, and nanodrops of water with a content of $(5.0 \pm 0.2)\%$ by weight, measured at measurement temperatures from 293.15 to 333.15 K. Supply voltage $V_{DC} = 100$ V.
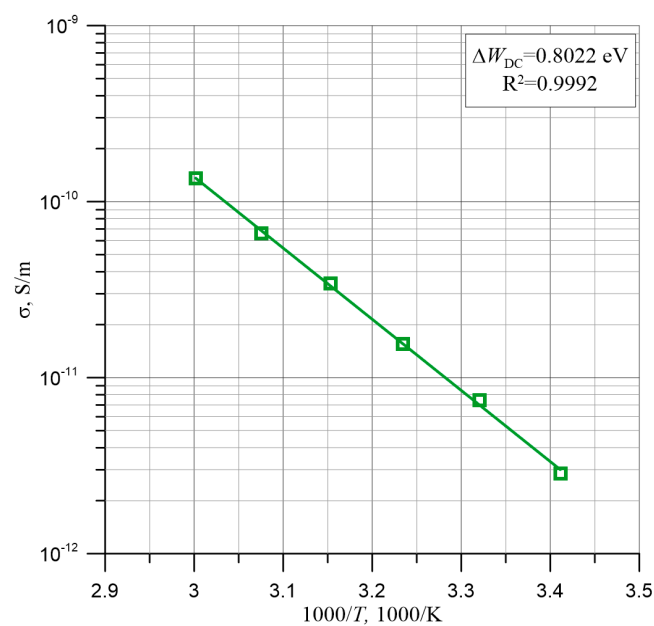

Figure 3. Dependence of DC conductivity on inverse temperature.

Figure 4 shows, in the form of points, the experimental results of the alternating current conductivity values of the composite of cellulose, insulating oil, and water nanoparticles for its content $(5.0 \pm 0.2)\%$ by weight, measured at measurement temperatures from 293.15

to 333.15 K with a step of 8 K. The figure shows that in the ultra-low frequency area, the value of alternating current conductivity is a constant value. This value increases as the temperature increases. This means that in this frequency area the value of alternating current conductivity depends only on temperature and not on the relaxation time. With a further increase in frequency, the value of the alternating current conductivity starts to increase. The beginning of the increase moves as the temperature increases to the higher frequency area. This is related to the change in the relaxation time as the temperature increases, as described by formula (13). For a precise calculation of the activation energy of the relaxation time and the conductivity, conductivity values between adjacent measuring points are needed. Polynomial approximation was used to determine the intermediate values between adjacent test points. The approximation of experimental waveforms was performed using the method proposed in paper [29]. In Figure 4, the approximation results are presented as continuous lines. Each of these lines consists of 200 points per decade, obtained by polynomial approximation. The values of R^2 for the approximated courses are very close to unity (Table 1).
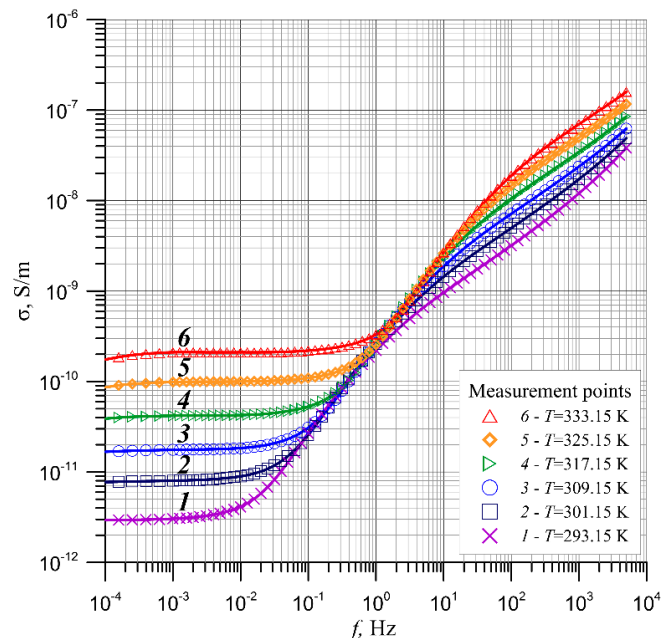

Figure 4. Frequency dependence of alternating current conductivity of a composite of cellulose, transformer oil, and water nanoparticles for its content (5.0 $\pm$ 0.2)% by weight measured at measurement temperatures from 293.15 to 333.15 K. Continuous lines—polynomial approximation.

Table 1. Values of R^2 and the position of the f_{max} maxima of the frequency factor $\alpha_{max}(f)$ for the approximation of the polynomial alternating current conductivity for different measurement temperatures.

T, K	293.15	301.15	309.15	317.15	325.15	333.15
R^2, a.u.	0.9999989	0.9999992	0.9999995	0.9999997	0.9999999	0.9999998
f_{max}, Hz	0.08128	0.2239	0.5012	1.1749	2.6915	5.495

Figure 5 shows the percentage differences between the approximation waveforms and experimental results of alternating current conductivity. Figure 5 shows that the highest of the differences occurring in the low frequency area does not exceed 0.5%. The remaining differences are smaller and decrease with increasing frequency. This means a very high quality of polynomial approximation performed according to the method proposed in the paper [29].
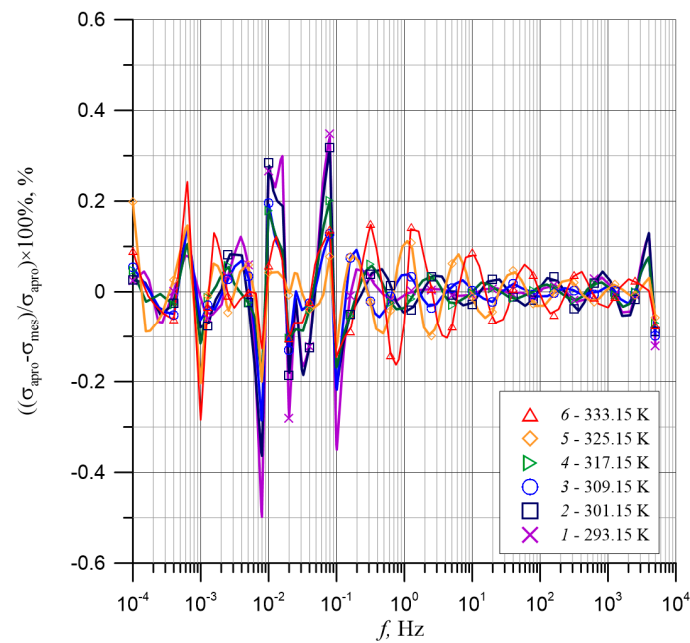
Figure 5. Percentage differences between experimental results of alternating current conductivity for a composite of cellulose, transformer oil, and water nanoparticles for measurement temperatures from 293.15 to 333.15 K and the results of approximation.

In Figure 6, derivative values of $d(\log\sigma)/d(\log f)$, obtained by differentiation of approximating courses presented in Figure 4, are presented. The figure shows that with the increase in frequency, an increase in derivative value is observed practically from zero to the maximum. Then the value of the derivative decreases and reaches the minimum. Further increase in frequency leads to the increase in the derivative value and reaching the next maximum.
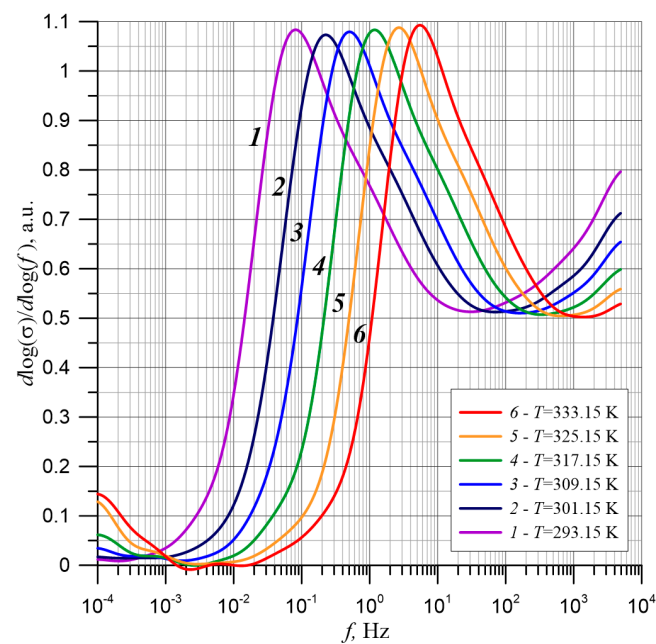

Figure 6. Dependence of the derivative logarithm of conductivity on the frequency logarithm for a composite of cellulose, transformer oil, and water nanoparticles with moisture content $(5.0 \pm 0.2)\%$ by weight for measurement temperatures from 293.15 to 333.15 K.

We now compare the experimental dependence of direct and alternating current conductivity with the model of hopping conductivity (electron tunneling) at direct and alternating current, discussed in Section 2. Figure 7 shows the value of DC conductivity in the form of a horizontal dotted line and frequency dependence of alternating current conductivity and frequency factor $\alpha(f)$ determined at measuring temperature 293.15 K.
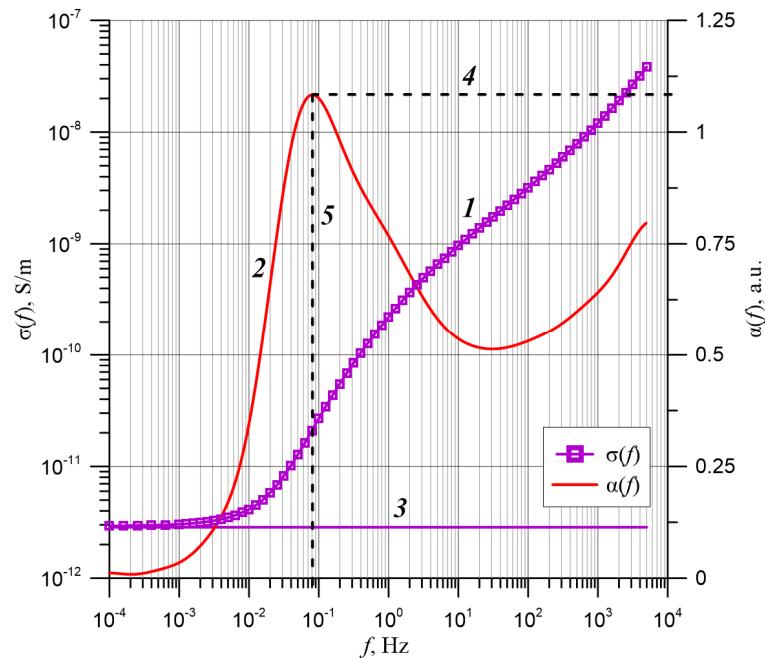

Figure 7. Frequency dependence of alternating current conductivity 1 and frequency factor $\alpha(f)$—2 for a composite of cellulose, transformer oil, and water nanoparticles for measurement temperature 293.15 K: 3—DC conductivity value, 4—maximum value of factor $\alpha_{max}(f)$, 5—frequency f_{max} at which $\alpha_{max}(f_{max})$ occurs.

The first of the conclusions of the model is the equality of DC and AC conductivity, measured in the ultra-low frequency area. Figure 7 shows that this condition is fulfilled. It also follows from the model that, with the increase in frequency, the alternating current conductivity starts to increase faster (Figure 1a). The frequency factor $\alpha_{(f)}$, which determines the rate of increase in conductivity, described by formula (20), starts to increase from zero in the ultra-low frequency area, where $\sigma(f)$ = const. At the point of the fastest increase in conductivity, coefficient $\alpha_{(f)}$ obtains a maximum value of $\alpha_{max}(fmax)$. With a further increase in frequency, the rate of increase in conductivity decreases and the coefficient $\alpha_{(f)}$ decreases its value. A comparison of the experimental waveforms of alternating current conductivity and the frequency factor $\alpha_{(f)}$ (Figure 7) with the waveforms defined in the model (Figure 1a,b) shows that the experimental waveforms and those calculated on the basis of the model perfectly match. This means that the frequency dependence of alternating current conductivity and frequency factor $\alpha_{(f)}$, in addition to the equality of direct current conductivity and low frequency alternating current conductivity values, indicate the presence in the composite of cellulose, transformer oil, and water nanoparticles of hopping conductivity, based on the quantum-mechanical electron tunneling phenomenon.

On the basis of comparison of experimental and numerically calculated waveforms for the value $\alpha_{(f)}$, we can determine the expected values of relaxation times occurring for different temperatures in the frequency range from 10^{-1} to 101 Hz. From the diagrams shown in Figure 6, the values of $f_{max}(T)$ frequencies at which $\alpha_{max}(f)$ occurs for different temperatures were determined. These values are shown in Table 1. The values of $\alpha_{max}(fmax)$ for the different measuring temperatures (Figure 6) are within the limits of $\alpha_{max}(f) \approx$ (1.08 ± 0.01). The value of $f_{max} \cdot \tau m \approx$ (0.0417 ± 0.0003) was determined from the simulation waveforms shown in Figure 1b. By substituting the values of $f_{max}(T)$ given in Table 1 and

$f_{max} \cdot \tau m$ for formula (25), the temperature dependence of the expected relaxation time value $\tau m(T)$ was calculated. Based on the obtained values of $\tau m(T)$, an Arrhenius diagram was drawn up, shown in Figure 8.
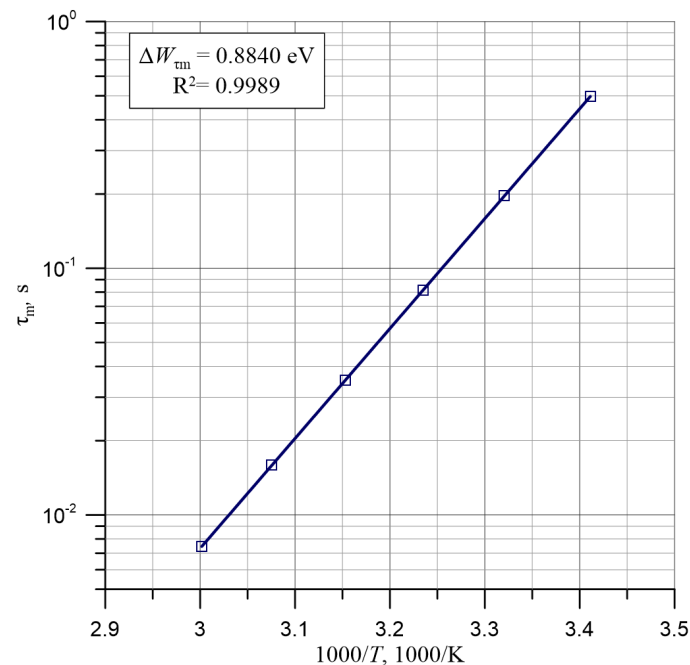

Figure 8. Arrhenius diagram for the value of the expected relaxation time.

The approximation, made using the method of the smallest squares, showed that it is a linear dependence. The coefficient of determination $R^2 = 0.9989$, which is very close to unity, proves a very high quality of approximation. On the basis of the obtained approximation formula, the activation energy of the value of expected relaxation time was determined, and amounted to $\Delta W \tau m \approx (0.884 \pm 0.0203)$ eV.

The resulting uncertainty value of the relaxation time activation energy is $\pm 2.3\%$, which is a satisfactory value.

Figures 6 and 7 show that with a further increase in frequency, the value $\alpha(f)$ decreases to a minimum, which, depending on the temperature, is in the frequency range from 10 to 103 Hz. After passing through the minimum, the value $\alpha_{(f)}$ starts to increase, striving for the next maximum. This is indicated by a slowdown in the rate of increase in $\alpha_{(f)}$ for a temperature of 293.15 K, which can be seen in the frequency range near 5000 Hz. The position of the second maximum is outside the frequency range used in the Dirana PDC-FDS. Therefore, it was not possible to determine the position of the second maximum, the value of the expected relaxation time, or the activation energy. The increase in $\alpha_{(f)}$ after passing through the minimum and aiming at the second maximum indicate the occurrence of two electron tunneling mechanisms in the pressboard, which differ in their values of expected relaxation times.

The location of alternating current conductivity in double logarithmic coordinates is influenced simultaneously by two factors. One of these is the activation energy of alternating current conductivity and the other is the activation energy of relaxation time. The influence of the activation energy of alternating current conductivity is that the relationship moves vertically as the temperature increases. This is clearly visible in the ultra-low frequency area (DC conductivity). Changes in the relaxation time, the value of which is determined by the temperature and the activation energy, result in a shift in the higher frequencies along the vertical axis as the temperature increases. According to the DC and AC hopping conductivity model in the ultra-low frequency area, the conductivity is a constant value and does not depend on frequency (formula (17)). Figure 4 shows that in the ultra-low

frequency area, the experimental value of conductivity does not depend on the frequency but increases with temperature.

Figure 9 shows the Arrhenius diagram for conductivity at frequencies 10^{-4} Hz, i.e., in the range where the conductivity value does not depend on frequency. Linear approximation of experimental values by the method of smallest squares showed its very high accuracy. This is evidenced by the value of the coefficient of determination $R^2 = 0.9998$, which is very close to unity. This indicates the constancy of the energy of activation of the conductivity over the whole temperature range. On the basis of the approximation formula, the value of activation energy of the low-frequency conductivity $\Delta W\sigma = 0.8575$ eV was determined.
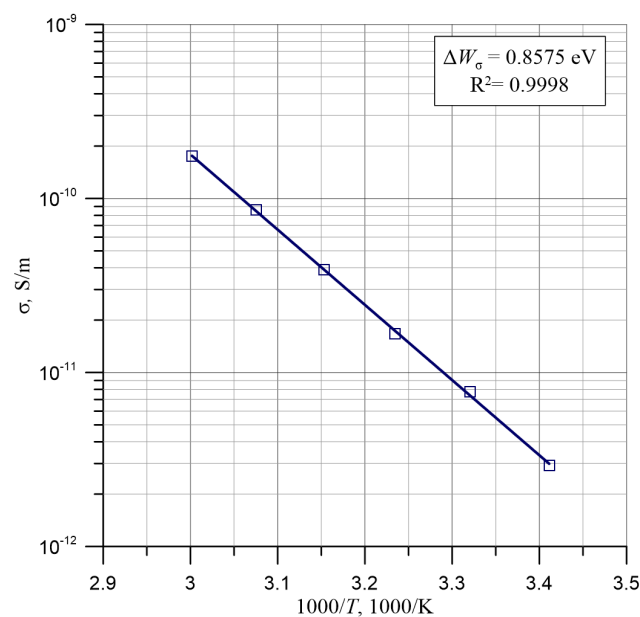

Figure 9. Arrhenius diagram for conductivity at 10^{-4} Hz.

The fact that, in the ultra-low frequency area, the conductivity value does not depend on the value of relaxation time allows the influence of the activation energy of the conductivity on the course of the conductivity to be eliminated. In order to eliminate the influence of the activation energy of the conductivity, the $\sigma_{(f)}$ waveforms measured at temperatures from 301.15 to 333.15 K are shifted along the vertical axis to 293.15 K, which is the reference temperature in electrical engineering. The shifts are made in such a way that the conductivities at 10^{-4} Hz overlap. The alternating current conductivity waveforms shifted along the vertical axis are shown in Figure 10. After the shift to alternating current conductivity waveforms shown in Figure 10, only the temperature dependence of relaxation time of the conductivity is affected.

In Figure 10, the horizontal dotted lines indicate the range from 10^{-11} to 2×10^{-9} S/m, which contains the growth segments of the shifted conductivity waveforms for all measurement temperatures. In this area, 22 conductivity values were selected, from which the values of the activation energy of relaxation time were determined. Such a large number of conductivity values were selected to increase the accuracy of the determination of the average value of the activation time energy of the conductivity and the uncertainty of its measurement. For each of the 22 conductivity values from the waveforms shown in Figure 10, the frequency values at which the selected conductivity value occurs were determined for the different measurement temperatures. These values were used to draw the Arrhenius diagrams presented in Figure 11. The smallest squares were used to approximate the Arrhenius diagrams. These are linear relationships. Their high accuracy is indicated by the values of determination coefficients R^2, which were very close to unity, presented in Table 2. The lowest of $R^2 = 0.9992$ and the mean value $R^2 \approx (0.9996 \pm 0.00022)$. On the basis

of the approximation formulas obtained, 22 values of the activation energy of relaxation time of the conductivity were determined, presented in Table 2.
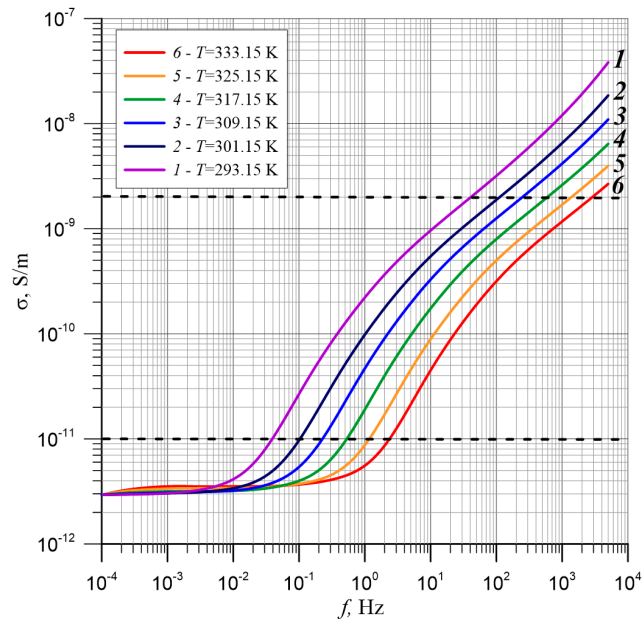

Figure 10. Frequency dependence of the conductivity of a composite of cellulose, transformer oil, and water nanoparticles measured at measurement temperatures from 293.15 to 333.15 K shifted at 10^{-4} Hz to the conductivity value at 293.15 K.
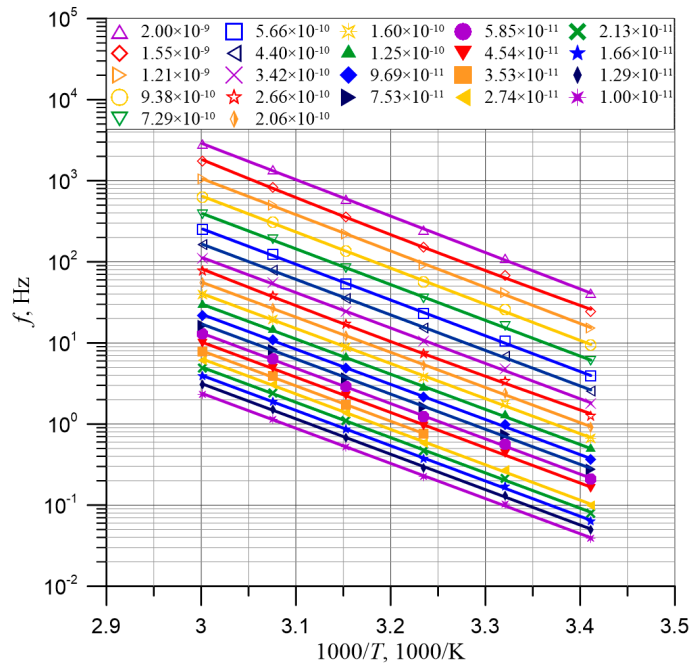

Figure 11. Arrhenius diagrams for 22 conductivity values from 10^{-11} to 2.00×10^{-9} S/m, on the basis of which the values of activation energy of relaxation time of the conductivity $\Delta W_{\tau\sigma}$.

Table 2. Activation energies of relaxation time of the conductivity $\Delta W_{\tau\sigma}$ and R^2 values for the 22 linear approximations of Arrhenius diagrams shown in Figure 11.

σ, S/m	$\Delta W_{\tau\sigma}$, eV	R^2, a.u.
1.00×10^{-11}	0.860	0.9998
1.29×10^{-11}	0.866	0.9998
1.66×10^{-11}	0.864	0.9998
2.13×10^{-11}	0.864	0.9998
2.74×10^{-11}	0.866	0.9993
3.53×10^{-11}	0.860	0.9995
4.54×10^{-11}	0.864	0.9998
5.85×10^{-11}	0.864	0.9998
7.53×10^{-11}	0.860	0.9995
9.69×10^{-11}	0.860	0.9995
1.25×10^{-10}	0.860	0.9998
1.60×10^{-10}	0.858	0.9999
2.06×10^{-10}	0.860	0.9998
2.66×10^{-10}	0.863	0.9998
3.42×10^{-10}	0.866	0.9993
4.40×10^{-10}	0.869	0.9993
5.66×10^{-10}	0.875	0.9992
7.29×10^{-10}	0.875	0.9996
9.38×10^{-10}	0.885	0.9995
1.21×10^{-9}	0.888	0.9998
1.55×10^{-9}	0.893	0.9997
2.00×10^{-9}	0.892	0.9993
Average value	0.869	0.9996
Standard deviation	0.0107	0.00022

In Figure 12, 22 values for the activation energy of relaxation time of the conductivity are shown. The figure shows that the value of the activation energy of relaxation time of the conductivity is a constant value over a wide range of conductivity changes. Only in the highest frequency area 4 do the values slightly exceed the mean value + standard deviation. This may be due to an increase in uncertainty at the ends of the measuring range for many measuring instruments. The mean value of the activation energy of relaxation time of the conductivity is $\Delta W\tau\sigma \approx (0.869 \pm 0.0107)$ eV. Even the highest value at the end of the range, at 5000 Hz, is only 2.65% higher than the average value. From Table 2 and Figure 12 it can be seen that using 22 conductivity values to determine the average value of the activation energy of relaxation time of the conductivity allowed high accuracy to be obtained. The uncertainty of determining the activation energy of relaxation time is only ±1.23%. Comparing the values of $\Delta W\tau\sigma$ with $\Delta W\tau m \approx (0.884 \pm 0.0106)$ eV, obtained from directly determined values of relaxation times (Figure 8), shows that both values are identical within the limits of the uncertainty of their determination, and the difference between them is 1.7%.
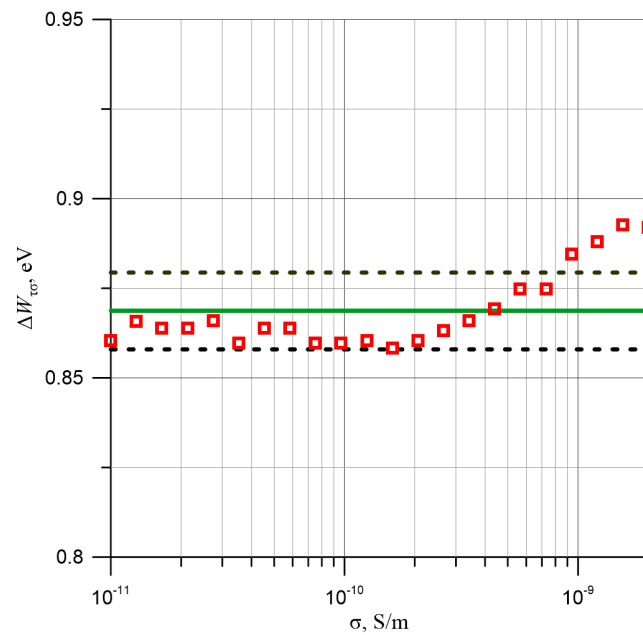
Figure 12. Dependences of the activation energy of relaxation time of the conductivity for 22 selected conductivity values from 10^{-11} to 2×10^{-9} S/m, mean value and mean value $\pm$ standard deviation.

5. Determination of Activation Energy of the Conductivity

After obtaining the activation energy of relaxation time of the conductivity, we can use its value to eliminate the influence of the relaxation time on the position of the frequency dependence of the conductivity shown in Figure 4. For this purpose, using the value $\Delta W\tau\sigma$, the waveforms from Figure 4 obtained for temperatures from 301.15 to 333.15 K were converted to a reference temperature of 293.15 K by moving them along the horizontal axis. The results of the conversion are shown in Figure 13. Figure 13 shows that the waveforms for frequencies 10^{-4} Hz and above are practically parallel.
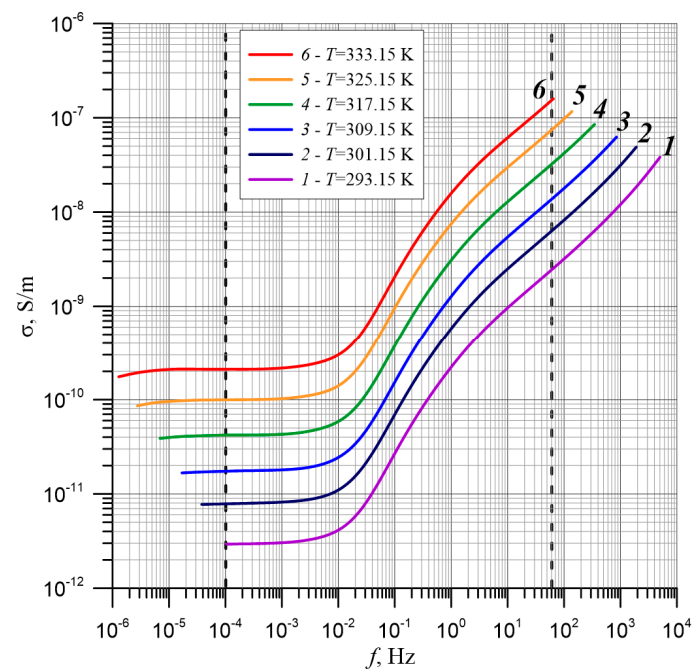

Figure 13. Frequency dependence of the conductivity of a composite of cellulose, mineral oil, and water nanoparticles measured at temperatures from 293.15 to 333.15 K, shifted by means of the activation energy of relaxation time of the conductivity to reference temperature 293.15 K.

This is evidenced by the differences between the frequency dependence of the conductivity for the reference temperature 293.15 K and the dependence for the other temperatures, as shown in Figure 14. From the figure it can be seen that the differences between the individual curves, when shifted with the activation energy of relaxation time of the conductivity, are horizontal lines that are very close to straight lines.
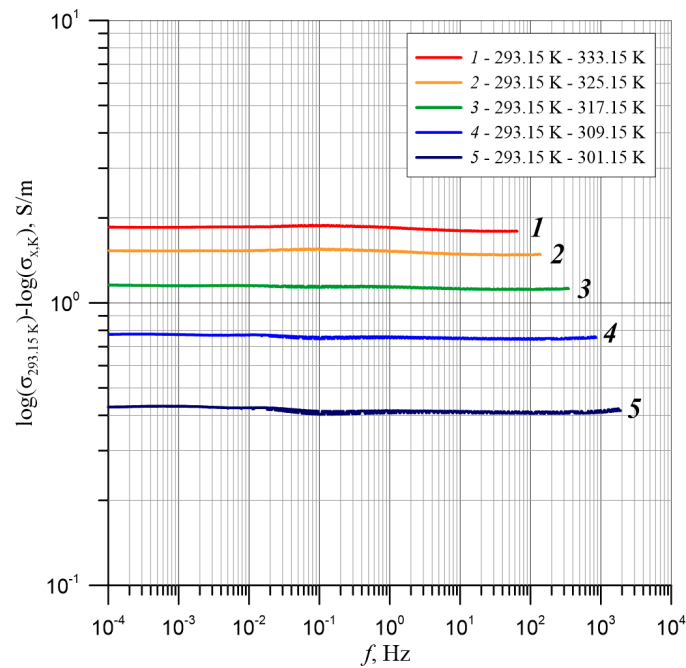

Figure 14. Differences between the frequency dependence of the conductivity for the reference temperature 293.15 K and the other temperatures shifted by the activation energy of relaxation time of the conductivity along the horizontal axis to the reference temperature 293.15 K.

The values of all six curves after shifting at the same time are within the frequency range from 10^{-4} to 60 Hz, indicated in Figure 13 by dashed vertical lines. As in the activation energy of relaxation time calculation cases described above, 22 points on the frequency axis were selected in the frequency range 10^{-4} to 60 Hz. For each of these points, conductivity values at different temperatures were determined. On this basis, 22 Arrhenius diagrams, shown in Figure 15, were drawn. This allows the average value of the activation energy of the conductivity and the uncertainty of its measurement to be determined with high accuracy. For the experimental points, the linear functions were approximated by the least squares method, presented in Figure 15 in the form of straight lines. The quality of the approximations is very high. The values of the coefficients of determination R^2, presented in Table 3, are between 0.9995 and 0.9999, and their mean value is (0.9997 ± 0.00011). On the basis of the obtained approximation formulas, 22 values of activation energy of the conductivity, presented in Table 3, were determined. The obtained average value of activation energy of the conductivity is $\Delta W\sigma \approx (0.894 \pm 0.0134)$ eV. The uncertainty of determining the activation energy of the conductivity is $\pm 1.50\%$.
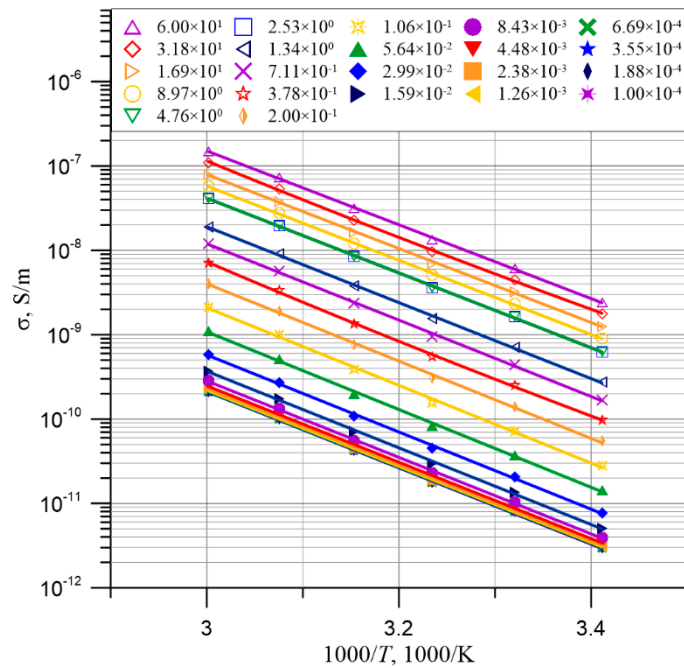
Figure 15. Arrhenius diagrams for 22 frequency values from 10^{-4} to 60 Hz, from which the activation energy of the conductivity values ΔW_σ were determined.

Table 3. Activation energy of the conductivity ΔW_σ and R^2 values for Arrhenius diagrams presented in Figure 16.

f, Hz	ΔW_σ, eV	R^2, a.u.
1.00×10^{-4}	0.898	0.9998
1.88×10^{-4}	0.896	0.9998
3.55×10^{-4}	0.895	0.9997
6.69×10^{-4}	0.895	0.9997
1.26×10^{-3}	0.896	0.9997
238×10^{-3}	0.898	0.9998
4.48×10^{-3}	0.899	0.9998
8.43×10^{-3}	0.900	0.9998
1.59×10^{-2}	0.902	0.9997
2.99×10^{-2}	0.907	0.9996
5.64×10^{-2}	0.915	0.9993
1.06×10^{-1}	0.914	0.9990
2.00×10^{-1}	0.910	0.9996
3.78×10^{-1}	0.905	0.9996
7.11×10^{-1}	0.899	0.9997
1.34×10^{0}	0.893	0.9995
2.53×10^{0}	0.886	0.9995
4.76×10^{0}	0.880	0.9999
8.97×10^{0}	0.873	0.9998
1.69×10^{1}	0.870	0.9998
3.18×10^{1}	0.871	0.9997
6.00×10^{1}	0.869	0.9998
Average value	0.894	0.9997
Standard deviation	0.0134	0.00019

Figure 16 shows the frequency dependence of the activation energy of the conductivity $\Delta W\sigma$ and the mean value $\pm$ standard deviation.

Figure 16 shows that activation energy of the conductivity value is a constant value over a wide frequency range. The greatest deviation from the average value occurs at 60 Hz and is only 2.8%. This is a highly satisfactory difference.
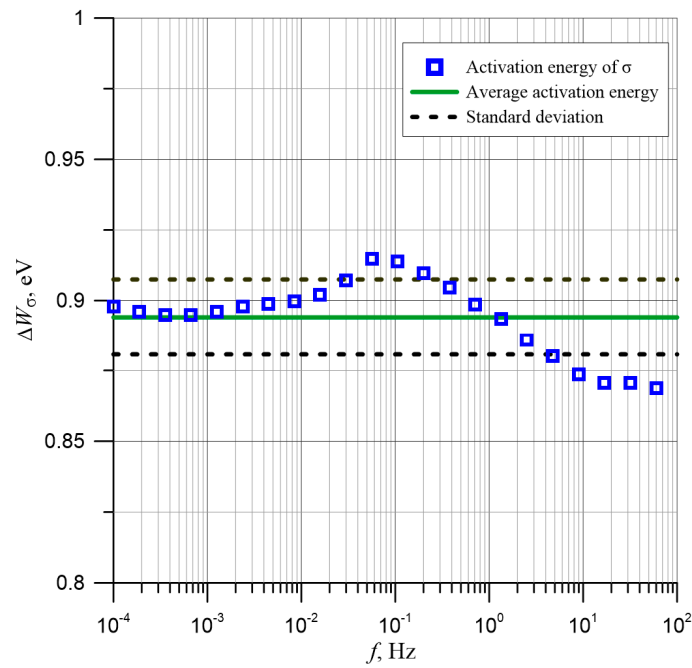

Figure 16. Frequency dependence for 22 values of activation energy of the conductivity for the composite of cellulose, synthetic ester, and water nanoparticles, mean value and mean value $\pm$ standard deviation.

The mean value of the activation energy of relaxation time of the conductivity is $\Delta W\tau\sigma \approx (0.869 \pm 0.0107)$ eV, and the activation energy of the conductivity is $\Delta W\sigma \approx (0.894 \pm 0.0134)$ eV. As can be seen, these values are very close. The difference between them is 0.025 eV. This means that the two activation energy values, describing the different processes in the composite of cellulose, mineral oil, and water nanoparticles, are equal within the error limits. The mean value and the standard deviation for the 44 residual activation energy values shown in Tables 2 and 3 is $\Delta W \approx (0.881 \pm 0.0140)$ eV. Due to the determination of such a large number of residual activation energy values, the uncertainty of determination is only $\pm 1.6\%$. This means that very high accuracy was achieved in determining the average value of activation energy.

Using the mean activation energy value $\Delta W \approx (0.881 \pm 0.0140)$ eV, the frequency dependence of the conductivity, obtained at different temperatures, was converted to a reference temperature of 293.15 K. The conversions were made by shifting the waveforms along the conductivity axis using formula (12) and the frequency using formula (20). The results of the conversion are shown in Figure 17.
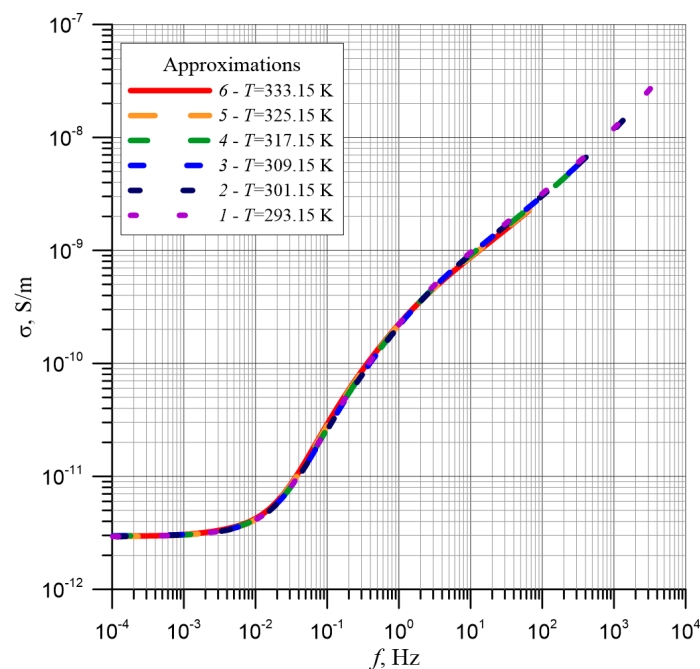
Figure 17. Frequency dependence of conductivity for measuring temperatures from 293.15 to 333.15 K shifted along the horizontal and vertical axes by means of activation energy ΔW to reference temperature 293.15 K.

From Figure 17, it can be seen that all six passages overlap perfectly. This means that the shape of the frequency dependence of the conductivity depends only on the parameters of the composite of the pressboard and mineral oil, and the moisture content of the pressboard. The position of each of the six waveforms in relation to the double logarithmic coordinates (Figure 4) is determined by the temperature. The influence of the temperature on the position of the waveforms is determined by the temperature dependence of the relaxation time of the conductivity. This moves the curves along the horizontal axis (frequency axis). The dependence of the conductivity value on temperature shifts the waveforms along the vertical axis (the conductivity axis). The simultaneous interaction of both of these dependencies determines the position of the waveform in relation to the coordinate axis.

6. Conclusions

To prepare a sample for laboratory tests, a method of moisturizing a pressboard impregnated with insulating oil, as close as possible to the moisturization of cellulose insulation in power transformers, was applied in the study. The previously dried and vacuum-impregnated moisture was delivered from moistened tiles. Moisture from these tiles was diffused into the oil, which supplied it to the vacuum-impregnated dry tile, by which it was absorbed. The tile moistening process was carried out over a year and a half. A sample of pressboard impregnated with insulating oil with water content $(5.0 \pm 0.2)\%$ by weight was prepared for measurements. A sample with such a high content was selected due to the fact that the accumulation of water in the transformer insulation to the level exceeding 5% by weight may cause a catastrophic failure of the transformer.

Precise tests of direct-current conductivity σDC and alternating-current $\sigma_{(f)}$ by the FDS method were performed on such a composite of cellulose, transformer oil, and water nanoparticles. Measurements were made in the temperature range from 293.15 to 333.15 K with a step of 8 K. The uncertainty of temperature maintenance during measurements was below ± 0.01 K.

For the analysis of the obtained results, the model of hopping conductivity on direct and alternating current was used, based on the quantum phenomenon of electron tunneling between the potential wells and nanodrops of water.

It was found that in the ultra-low frequency area the conductivity value depends on temperature and does not depend on frequency. With a further increase in frequency, the conductivity starts to increase. The beginning of the increase moves as the measuring temperature increases to the higher frequency area. This is related to the influence of temperature on the relaxation time of the conductivity. Based on the $d(\log\sigma)/d(\log f)$-derived waveforms, it was established that the increase in the conductivity value takes place in two stages. From the comparison of the experimental results of the maximum position of the derivative $d(\log\sigma)/d(\log f)$ for the first stage and the results of the computer simulation for the hopping conductivity model (electron tunneling), the temperature dependence of the expected relaxation time value of the conductivity was determined. The expected value of the activation energy of relaxation time $\Delta W\tau m \approx (0.884 \pm 0.0203)$ eV was determined. For the second stage, the derivative value reached a maximum in the frequency range above the upper range of the meter.

It was found that the position of relation $\sigma_{(f)}$ in double logarithmic coordinates is influenced by two factors simultaneously. The first is the temperature dependence of the conductivity, which is determined by the activation energy of the conductivity. This causes a shift along the vertical axis as the temperature increases. The second is the temperature dependence of the relaxation time of the conductivity. This is related to the activation energy of the relaxation time. This causes the waveforms to shift along the horizontal axis as the temperature rises to the higher frequencies. The simultaneous interaction of these two factors determines the position of the waveform $\sigma_{(f)}$ at a given temperature.

A comparison of the DC and AC conductivity measurements shows that these values are identical in the ultra-low frequency area. In this frequency area, the temperature only moves the conductivity value in a vertical direction. This eliminates the influence of the activation energy of the conductivity on the obtained $\sigma_{(f)}$. For this purpose, the relationships for temperatures 301.15 K and above were shifted along the vertical axis so that the conductivity values at 10^{-4} Hz were equal to the conductivity densities obtained at 293.15 K on this frequency.

After shifting in the area from 10^{-11} to 2×10^{-9} S/m, where all six curves at different measurement temperatures are simultaneously located, 22 conductivity values were selected. For these values Arrhenius charts were drawn, from which 22 values of the activation energy of the relaxation time of the conductivity were determined and the mean value $\Delta W\tau\sigma \approx (0.869 \pm 0.0107)$ eV.

Using the activation energy of relaxation time, the waveforms for temperatures 301.15 K and higher were shifted to 293.15 K. This eliminated the effect of the relaxation time. After the shift, all six curves for different temperatures were in the frequency range of 10^{-4} to 60 Hz. In this range, 22 points on the frequency axis were selected. For each of these points, conductivity values at different temperatures were determined and 22 Arrhenius diagrams were drawn, from which 22 values of activation energy of the conductivity were determined. The average value of the activation energy of the conductivity obtained on this basis was $\Delta W\sigma \approx (0.894 \pm 0.0134)$ eV.

It was found that the values of the activation energy of the relaxation time of the conductivity and the activation energy of the conductivity are equal within the limits of uncertainty, and the mean value was $\Delta W\sigma \approx (0.881 \pm 0.0140)$ eV. Using the mean value of activation energy, the frequency dependence of conductivity, obtained at different temperatures, was shifted to 293.15 K. For this purpose, first the waveforms were shifted along the horizontal and then the vertical axis.

For this purpose, the horizontal and vertical axes were first shifted, then the vertical axes. This means that the shape of the frequency dependence of the conductivity depends on the moisture content of the pressboard, impregnated with insulating oil. The position of each of the waveforms in relation to the double logarithmic coordinates is determined by

the temperature through the activation energy of relaxation time and the activation energy of the conductivity.

The paper proposes a way to precisely determine the standard characteristics for the conductivity of a pressboard impregnated with insulating oil and containing moisture. This method involves: the use of a large number of measuring points in the area of low and ultra-low frequencies; the use of a climatic chamber with an uncertainty of temperature determination of less than ±0.01 K; and determination of activation energy of conductivity and relaxation times with high accuracy. The application of such a method of determination of standard characteristics will allow the accuracy of determination of moisture content in cellulose insulation of power transformers to be improved, particularly in the range close to 5% of weight.

Author Contributions: Conceptualization, P.Z., P.R. and T.N.K.; methodology, P.Z.; software, P.R. and K.K.; validation, P.Z. and P.R.; formal analysis, P.Z., P.R., T.N.K. and K.K.; investigation, P.R., K.K. and V.B.; resources, P.R., T.N.K., K.K. and V.B.; data curation, P.R., K.K. and V.B.; writing—original draft preparation, P.Z.; writing—review and editing, T.N.K. and K.K.; visualization, T.N.K.; supervision, P.Z.; funding acquisition, P.Z., P.R., T.N.K., K.K. and V.B. All authors have read and agreed to the published version of the manuscript.

Conflicts of Interest: The authors declare no conflict of interest. The funders had no role in the design of the study; in the collection, analyses, or interpretation of data; in the writing of the manuscript, or in the decision to publish the results.

References

1. Bezprozvannych, G.V.; Moskvitin, E.S.; Kyessaeyv, A.G. The absorption characteristics of the phase and zone paper-impregnated insulation of power cable at direct voltage. *Electr. Eng. Electromech.* **2015**, *5*, 63–68. [CrossRef]
2. Xie, Y.M.; Ruan, J.J. Parameters Identification and Application of Equivalent Circuit at Low Frequency of Oil-Paper Insulation in Transformer. *IEEE Access* **2020**, *8*, 86651–86658. [CrossRef]
3. Wolny, S.; Zdanowski, M. Analysis of recovery voltage parameters of paper-oil insulation obtained from simulation investigations using the Cole-Cole model. *IEEE Trans. Dielectr. Electr. Insul.* **2009**, *16*, 1676–1680. [CrossRef]
4. Saha, T.K.; Yao, Z.T. Experience with return voltage measurements for assessing insulation conditions in service-aged transformers. *IEEE Trans. Power Deliv.* **2003**, *18*, 128–135. [CrossRef]
5. Saha, T.K. Review of time-domain polarization measurements for assessing insulation condition in aged transformers. *IEEE Trans. Power Deliv.* **2003**, *18*, 1293–1301. [CrossRef]
6. Zainir, R.A.; Muhamad, N.A.; Adzis, Z.; Piah, M.A.M.; Kasri, N.F.; Jamail, N.A.M. RVM versus PDC Methods for Insulations' Conductivity and Moisture Content Monitoring. *J. Trknologi* **2013**, *64*, 49–53. [CrossRef]
7. Hao, J.; Liao, R.; Chen, G.; Ma, Z.; Yang, L. Quantitative analysis ageing status of natural ester-paper insulation and mineral oil-paper insulation by polarization/depolarization current. *IEEE Trans. Dielectr. Electr. Insul.* **2012**, *19*, 188–199.
8. Saha, T.K.; Purkait, P. Investigation of polarization and depolarization current measurements for the assessment of oil-paper insulation of aged transformers. *IEEE Trans. Dielectr. Electr. Insul.* **2004**, *11*, 144–154. [CrossRef]
9. Fofana, I.; Hemmatjou, H.; Meghnefi, F. Effect of thermal transient on the polarization and depolarization current measurements. *IEEE Trans. Dielectr. Electr. Insul.* **2011**, *18*, 513–520. [CrossRef]
10. Ambrozevich, S.A.; Sibatov, R.T.; Uchaikin, D.V.; Morozova, E.V. To a Method of Polarization-Depolarization Currents for Diagnosis of Dielectric Isolation. *Russ. Phys. J.* **2016**, *58*, 1284–1290. [CrossRef]
11. Ekanayake, C.; Gubanski, S.M.; Graczkowski, A.; Walczak, K. Frequency Response of Oil Impregnated Pressboard and Paper Samples for Estimating Moisture in Transformer Insulation. *IEEE Trans. Power Deliv.* **2006**, *21*, 1309–1317. [CrossRef]
12. Setayeshmehr, A.; Fofana, I.; Eichler, C.; Akbari, A.; Borsi, H.; Gockenbach, E. Dielectric spectroscopic measurements on transformer oil-paper insulation under controlled laboratory conditions. *IEEE Trans. Dielectr. Electr. Insul.* **2008**, *15*, 1100–1111. [CrossRef]
13. Fofana, I.; Hemmatjou, H.; Meghnefi, F.; Farzaneh, M.; Setayeshmehr, A.; Borsi, H.; Gockenbach, E. On the frequency domain dielectric response of oil-paper insulation at low temperatures. *IEEE Trans. Dielectr. Electr. Insul.* **2010**, *17*, 799–807. [CrossRef]
14. Mousavi, S.A.; Sedighizadeh, M.; Hekmati, A.; Bigdeli, M. Artificial neural network based method for temperature correction in FDS measurement of transformer insulation. *J. Phys. D Appl. Phys.* **2020**, *53*, 145103. [CrossRef]

15. Wang, D.Y.; Zhou, L.J.; Liao, W.; Wang, A.; Xu, X.W.; Guo, L. Moisture estimation for oil-immersed bushing based on FDS method: Field application. *IET Gener. Transm. Distrib.* **2018**, *12*, 2762–2769. [CrossRef]

16. Wang, L.H.; Yin, F.; Shen, Y.; Tang, C. Reactive molecular dynamics research on influences of water on aging characteristics of PMIA insulation paper. *J. Appl. Phys.* **2020**, *127*, 105107. [CrossRef]

17. Zhang, T.; Wang, S.; Zhang, C.; Abu-Siada, A.; Li, L.D.; Han, J.W.; Du, Z.B. Investigating a New Approach for Moisture Assessment of Transformer Insulation System. *IEEE Access* **2020**, *8*, 81458–81467. [CrossRef]

18. Zhang, M.; Liu, J.; Lv, J.; Chen, Q.; Qi, P.; Sun, Y.; Jia, H.; Chen, X. Improved method for measuring moisture content of mineral-oil-impregnated cellulose pressboard based on dielectric response. *Cellulose* **2018**, *25*, 5611–5622. [CrossRef]

19. Liu, J.F.; Fan, X.H.; Zhang, Y.Y.; Zhang, C.H.; Wang, Z.X. Aging evaluation and moisture prediction of oil-immersed cellulose insulation in field transformer using frequency domain spectroscopy and aging kinetics model. *Cellulose* **2020**, *27*, 7175–7189. [CrossRef]

20. Liu, J.F.; Fan, X.H.; Zhang, Y.Y.; Zheng, H.B.; Zhu, M.Z. Quantitative evaluation for moisture content of cellulose insulation material in paper/oil system based on frequency dielectric modulus technique. *Cellulose* **2020**, *27*, 2343–2356. [CrossRef]

21. Krause, C. Power transformer insulation—History, technology and design. *IEEE Trans. Dielectr. Electr. Insul.* **2012**, *19*, 1941–1947. [CrossRef]

22. Zhang, J.; Zhang, B.; Fan, M.; Wang, L.; Ding, G.; Tian, Y.; Chen, Q. Effects of external radiation heat flux on combustion characteristics of pure and oil-impregnated transformer insulating paperboard. *Process. Saf. Prog.* **2018**, *37*, 362–368. [CrossRef]

23. Li, H.; Zhong, L.; Yu, Q.; Mori, S.; Yamada, S. The resistivity of oil and oil-impregnated pressboard varies with temperature and electric field strength. *IEEE Trans. Dielectr. Electr. Insul.* **2014**, *21*, 1851–1856. [CrossRef]

24. Kouassi, K.; Fofana, I.; Cissé, L.; Hadjadj, Y.; Yapi, K.; Diby, K. Impact of Low Molecular Weight Acids on Oil Impregnated Paper Insulation Degradation. *Energies* **2018**, *11*, 1465. [CrossRef]

25. Żukowski, P.; Kołtunowicz, T.N.; Kierczyński, K.; Subocz, J.; Szrot, M. Formation of water nanodrops in cellulose impregnated with insulating oil. *Cellulose* **2015**, *22*, 861–866. [CrossRef]

26. Baird, P.J.; Herman, H.; Stevens, G.C.; Jarman, P.N. Spectroscopic measurement and analysis of water and oil in transformer insulating paper. *IEEE Trans. Dielectr. Electr. Insul.* **2006**, *13*, 293–308. [CrossRef]

27. Wolny, S. The influence of thermal degradation of aramid paper on the polarization mechanisms oil-impregnated insulation in high frequency domain. *Prz. Elektrotechniczny* **2018**, *94*, 105–107.

28. Graczkowski, A. Dielectric response of cellulose impregnated with different insulating liquids. *Prz. Elektrotechniczny* **2010**, *86*, 223–225.

29. Żukowski, P.; Kołtunowicz, T.N.; Kierczyński, K.; Subocz, J.; Szrot, M.; Gutten, M.; Sebok, M.; Jurcik, J. An analysis of AC conductivity in moist oil-impregnated insulation pressboard. *IEEE Trans. Dielectr. Electr. Insul.* **2015**, *22*, 2156–2164. [CrossRef]

30. Rahman, M.F.; Nirgude, P. Partial discharge behaviour due to irregular-shaped copper particles in transformer oil with a different moisture content of pressboard barrier under uniform field. *IET Gener. Transm. Distrib.* **2019**, *13*, 5550–5560. [CrossRef]

31. Hill, J.; Wang, Z.D.; Liu, Q.; Krause, C.; Wilson, G. Analysing the power transformer temperature limitation for avoidance of bubble formation. *High. Volt.* **2019**, *4*, 210–216. [CrossRef]

32. Garcia, B.; Villarroel, R.; Garcia, D. A Multiphysical Model to Study Moisture Dynamics in Transformers. *IEEE Trans. Power Deliv.* **2019**, *34*, 1365–1373. [CrossRef]

33. Landau, L.D.; Lifshits, E.M.; Pitaevskiĭ, L.P. *Electrodynamics of Continuous Media*; Pergamon: New York, NY, USA, 1984.

34. Zukowski, P.; Koltunowicz, T.N.; Boiko, O.; Bondariev, V.; Czarnacka, K.; Fedotova, J.A.; Fedotov, A.K.; Svito, I.A. Impedance model of metal-dielectric nanocomposites produced by ion-beam sputtering in vacuum conditions and its experimental verification for thin films of $(FeCoZr)_x(PZT)_{(100-x)}$. *Vacuum* **2015**, *120*, 37–43. [CrossRef]

35. Kołtunowicz, T.N.; Bondariev, V.; Żukowski, P.; Fedotova, J.A.; Fedotov, A.K. AC electrical resonances in nanocomposites with partly oxidized FeCoZr grains embedded in CaF_2 ceramic matrix-effects of annealing. *J. Alloy. Compd.* **2020**, *819*, 153361. [CrossRef]

36. Svito, I.A.; Fedotov, A.K.; Saad, A.; Zukowski, P.; Koltunowicz, T.N. Influence of oxide matrix on electron transport in $(FeCoZr)_x(Al_2O_3)_{1-x}$ nanocomposite films. *J. Alloy. Compd.* **2017**, *699*, 818–823. [CrossRef]

37. Żukowski, P.; Kierczyński, K.; Kołtunowicz, T.N.; Rogalski, P.; Subocz, J. Application of elements of quantum mechanics in analysing AC conductivity and determining the dimensions of water nanodrops in the composite of cellulose and mineral oil. *Cellulose* **2019**, *26*, 2969–2985. [CrossRef]

38. Waygood, A. *An Introduction to Electrical Science*, 2nd ed.; Routledge: New York, NY, USA, 2019.

39. Mott, N.F.; Davis, E.A. *Electronic Processes in Non-Crystalline Materials*; Claredon Press: Oxford, UK, 1979.

40. Tauc, J. *Amorphous and Liquid Semiconductors*; Plenum Press: London, UK, 1974; pp. 183–190.

41. Shklovskii, B.I.; Efros, A.L. *Electronic Properties of Doped Semiconductors*; Springer: Heidelberg, Germany, 1984.

42. Mott, N.F.; Gurney, R.W. *Electronic Processes in Ionic Crystals*; Clarendon Press: Oxford, UK, 1948.

43. Citroni, R.; Di Paolo, F.; Di Carlo, A. Replacing noble metals with alternative metals in MID-IR frequency: A theoretical approach. *AIP Conf. Proc.* **2018**, *1990*, 020004.

44. Żukowski, P.; Kołtunowicz, T.N.; Kierczyński, K.; Rogalski, P.; Subocz, J.; Szrot, M.; Gutten, M.; Sebok, M.; Jurcik, J. Permittivity of a composite of cellulose, mineral oil, and water nanoparticles: Theoretical assumptions. *Cellulose* **2016**, *23*, 175–183. [CrossRef]

45. Żukowski, P.; Kołtunowicz, T.N.; Kierczyński, K.; Rogalski, P.; Subocz, J.; Szrot, M.; Gutten, M.; Sebok, M.; Korenciak, D. Dielectric losses in the composite cellulose–mineral oil–water nanoparticles: Theoretical assumptions. *Cellulose* **2016**, *23*, 1609–1616. [CrossRef]

46. Nowak, R. *Statystyka dla Fizyków*; Państwowe Wydawnictwo Naukowe PWN: Warsaw, Poland, 2002.

47. Oommen, T.V. Moisture Equilibrium in Paper Oil Systems. In Proceedings of the 16th Electrical Insulation Conference, Chicago, IL, USA, 3–6 October 1983; pp. 162–166.

48. Rogalski, P. Measurement Stand, Method and Results of Composite Electrotechnical Pressboard-Mineral Oil Electrical Measurements. *Devices Methods Meas.* **2020**, *11*, 187–195. [CrossRef]

49. Zukowski, P.; Rogalski, P.; Koltunowicz, T.N.; Kierczynski, K.; Subocz, J.; Zenker, M. Cellulose Ester Insulation of Power Transformers: Researching the Influence of Moisture on the Phase Shift Angle and Admittance. *Energies* **2020**, *13*, 5511. [CrossRef]

50. Zaengl, W.S. Applications of dielectric spectroscopy in time and frequency domain for HV power equipment. *IEEE Electr. Insul. Mag.* **2003**, *19*, 9–22. [CrossRef]

51. Jadav, R.B.; Ekanayake, C.; Saha, T.K. Understanding the impact of moisture and ageing of transformer insulation on frequency domain spectroscopy. *IEEE Trans. Dielectr. Electr. Insul.* **2014**, *21*, 369–379. [CrossRef]

52. Gielniak, J.; Graczkowski, A.; Moranda, H.; Przybylek, P.; Walczak, K.; Nadolny, Z.; Moscicka-Grzesiak, H.; Feser, K.; Gubanski, S. Moisture in cellulose insulation of power transformers-statistics. *IEEE Trans. Dielectr. Electr. Insul.* **2013**, *20*, 982–987. [CrossRef]

53. Kornatowski, E.; Banaszak, S. Frequency Response Quality Index for Assessing the Mechanical Condition of Transformer Windings. *Energies* **2019**, *13*, 29. [CrossRef]

54. Piotrowski, T.; Rozga, P.; Kozak, R. Comparative Analysis of the Results of Diagnostic Measurements with an Internal Inspection of Oil-Filled Power Transformers. *Energies* **2019**, *12*, 2155. [CrossRef]

55. Hashemnia, N.; Abu-Siada, A.; Islam, S. Detection of power transformer bushing faults and oil degradation using frequency response analysis. *IEEE Trans. Dielectr. Electr. Insul.* **2016**, *23*, 222–229. [CrossRef]

56. Yousof, M.F.M.; Al-Ameri, S.; Ahmad, H.; Illias, H.A.; Arshad, S.N.M. A new approach for estimating insulation condition of field transformers using FRA. *Adv. Electr. Comput. Eng.* **2020**, *20*, 1–8.

57. Koch, M.; Tenbohlen, S.; Stirl, T. Diagnostic application of moisture equilibrium for power transformers. *IEEE Trans. Power Deliv.* **2010**, *25*, 2574–2581. [CrossRef]

58. Zaengl, W.S. Dielectric spectroscopy in time and frequency domain for HV power equipment, Part I: Theoretical considerations. *IEEE Electr. Insul. Mag.* **2003**, *19*, 5–19. [CrossRef]

59. Garcia, B.; Burgos, J.C.; Alonso, A.M.; Sanz, J. A moisture-in-oil model for power transformer monitoring—Part I: Theoretical foundation. *IEEE Trans. Power Deliv.* **2005**, *20*, 1417–1422. [CrossRef]

60. Martin, D.; Perkasa, C.; Lelekakis, N. Measuring Paper Water Content of Transformers: A New Approach Using Cellulose Isotherms in Nonequilibrium Conditions. *IEEE Trans. Power Deliv.* **2013**, *28*, 1433–1439. [CrossRef]

61. Oommen, T.V.; Prevost, T.A. Cellulose insulation in oil-filled power transformers: Part II maintaining insulation integrity and life. *IEEE Electr. Insul. Mag.* **2006**, *22*, 5–14. [CrossRef]